High resolution molecular line observations of the Serpens Nebula

Astron. Astrophys. 298, 594–605 (1995)

ASTRONOMY AND ASTROPHYSICS

High resolution molecular line observations of the Serpens Nebula

Glenn J. White[1], **Mark M. Casali**[2], **and Carlos Eiroa**[3]

[1] Department of Physics, Queen Mary and Westfield College, University of London, Mile End Road, London E1 4NS, England
[2] Royal Observatory, Blackford Hill, Edinburgh EH9 3HJ, England
[3] Departamento de Fisica Teorica, Facultad de Ciencias, Universitad Autonoma de Madrid, Cantoblanco E-28049 Madrid, Spain

Received 11 July 1994 / Accepted 21 November 1994

Abstract. The Serpens Molecular cloud is a nearby low / intermediate mass star forming region that is in the final stages of forming a densely packed cluster of stars. Spectra and high angular resolution maps of the CO, ^{13}CO, C^{18}O and C^{17}O $J = 2-1$ and CO $J = 4-3$ transitions were obtained to study the distribution of molecular gas near the cluster. These are supplemented with data on the $J = 4-3$ HCO$^+$ line (to probe the denser gas), and $^3P_1 - {}^3P_0$ line of atomic carbon. The mass of the region is estimated to be $\sim$ 1450 $M_\odot$, implying that the star formation efficiency in the region to date has been $\sim$ 2.5 percent. Several molecular outflows are visible in the maps; some are associated with compact objects visible in millimetre and submillimetre wave continuum maps, as well as more widespread diffuse high velocity gas that extends over much of the nebula. The mass and energy of material in the high velocity gas are relatively small, $\sim$ 0.3 $M_\odot$ and 3 x 10^{45} erg s^{-1}, consistent with the characteristics of outflows seen towards low mass star-formation regions. The directions of the overlapping outflow lobes do not however show a clear alignment with the cloud's large scale magnetic field as has been reported towards some other regions. The gas temperatures in the central part of the molecular cloud are warmer ($\sim$ 30 - 40 K) than typical for dark clouds, suggesting that the Serpens cluster has interacted with, and heated this gas. Estimates of the CO isotopomeric abundance ratios from these data may be strongly affected by opacity and radiative transfer effects. In a comparison of the LTE and LVG techniques, the disagreement between the derived column densities is discussed - with particular relevance to the higher rotational transitions.

Key words: star formation – ISM: Serpens Nebula – ISM: jets and outflows – radio lines: ISM

1. Introduction

The Serpens Molecular cloud is a nearby low / intermediate mass star formation region, which has been extensively studied at optical, near and far-infrared and millimetre wavelengths (Eiroa 1991). Near-IR images show a concentration of diffuse emission and cometary nebulosities, and a cluster of embedded pre-main sequence stars that are starting to emerge from the cloud (Eiroa & Casali 1992). This area has a remarkably high stellar density ($\geq$ 450 stars pc^{-3}), and a star formation efficiency suggested to be between 8 and 28 per cent (Eiroa & Casali 1992), implying that a bound cluster may be forming. More than 50 stars are associated with the region, which have a total luminosity and mass of $\sim$ 110 $L_\odot$ and $\sim$ 40 $M_\odot$ respectively, while far infrared data (Nordh et al. 1982; Harvey et al. 1984; Zhang et al. 1988; Eiroa & Casali 1992) show the total luminosity of the core region to be $\sim$ 84 - 210 $L_\odot$. The Serpens nebula lies in an extended molecular cloud, about 7 arc minutes west of the high mass star formation region S68 (Loren et al. 1979). It is associated with a triple radio continuum source that may be a proto-Herbig-Haro system at an early stage of evolution (Curiel et al. 1993). An extended molecular outflow reported by Bally & Lada (1983) may contain several superposed molecular outflows associated with the newly formed stars in the cluster (Eiroa et al. 1992). To search for the origins of the molecular outflow, and to compare the distribution of the outflow gas with near-IR and submillimetre continuum sources, we have made high angular resolution maps of the CO, ^{13}CO, C^{18}O and C^{17}O $J = 2 - 1$ and CO $J = 4 - 3$ transitions, supplemented with observations of the $J = 4 - 3$ HCO$^+$ line (to probe the denser gas), and finally maps in the $^3P_1 - {}^3P_0$ line of atomic carbon, CI. These data are used to study the inter isotopomeric abundance ratios of CO, and their variations with position and excitation within the cloud.

Send offprint requests to: Prof. Glenn J. White

2. Instrumentation

The $J = 2 - 1$ CO and isotopomeric data were obtained with the 15 metre James Clerk Maxwell Telescope in Hawaii during July 1992 and April 1993. The telescope efficiencies η_{fss} and η_{mb} were measured to be 0.77 and 0.63, and the beamsize was 21 arc seconds. These values of η_{fss} and η_{mb} were inferred from observations of the Moon, Jupiter and Mars, with corrections for atmospheric emission and gains in both sidebands. The ob-

servations were made during good atmospheric conditions, with pointing and tracking accuracy better than 2 arc seconds. The data were collected using an SIS receiver and acousto-optical spectrometer backend (White 1988), with a velocity resolution ~ 0.45 km s^{-1}. The data were calibrated in units of $T_r^* = T_a^* / \eta_{fss}$ using a standard chopper wheel calibration technique. The (0,0) position for the maps was at $\alpha(1950) = 18^h\ 27^m\ 25.4^s$, $\delta(1950) = +01^o\ 12'\ 16''$. A total of 292 CO, 219 ^{13}CO, 238 C^{18}O and 105 C^{17}O spectra were obtained (at rest frequencies of 230.538, 220.398, 219.56 and 224.714 GHz and rms noise values of ~ 0.2 K km s^{-1} for each respectively), sampled mostly on 20 arc second grids, with intermediate positions sampled on a 10" grid where the structure changed rapidly. The spectrum at the central (0,0) position was monitored frequently, and found to be reproducible to within ~ 5 percent. Several CO $J = 4 - 3$ spectra (461.0408 GHz - beamsize 10 arc seconds, $\eta_{mb} = 0.48$ and $\eta_{fss} = 0.68$, map grid size 10 arc seconds and rms noise level of ~ 2 K km s^{-1}) were obtained to compare with the $J = 2 - 1$ line shapes. To sample denser molecular gas and atomic gas, 81 HCO$^+$ $J = 4 - 3$ spectra (356.734 GHz - beamsize 15 arc seconds, $\eta_{fss} = 0.58$, map grid size 15 arc seconds and rms noise level of ~ 0.8 K km s^{-1}) and 74 spectra in the $^3P_1 - {}^3P_0$ atomic carbon CI line (492.160 GHz - beamsize 10 arc seconds, $\eta_{mb} = 0.46$ and $\eta_{fss} = 0.66$, map grid size 10 arc seconds and rms noise level of ~ 1 K km s^{-1}) were measured at selected positions close to CO peaks. It is worth emphasising the difficulty of accurately calibrating high frequency receivers on submillimetre telescopes (such as the JCMT) - the need for good atmospheric and tracking stability, and accurate correction for frequency and weather dependent atmospheric absorption require special care. The values of the 461 and 492 GHz efficiencies given above are averages of values obtained during the run from observations of several planets (Mars, Jupiter and Saturn) and of the Moon: they have an absolute uncertainty of $\pm$ 20 per cent - consistent with subsequent calibrations made during 1993 and early 1994. Despite considerable care and effort, it has proved difficult in practice to improve on this level of absolute calibration uncertainty.

3. The data

3.1. CO $J = 2 - 1$ data

The integrated CO $J = 2 - 1$ map in Fig. 1a shows a number of peaks lying close to the cluster of submillimetre wavelength continuum sources detected by Casali et al. (1993) - hereafter individual submillimetre sources will be designated SMM 'X', with X as indicated on Fig. 1g. Maps in the $J = 2 - 1$ ^{13}CO, C^{18}O and C^{17}O lines are shown in Figs. 1b, c and d.

The CO emission comes from three main regions, the complex in the SE of the map is associated with the main cluster of forming stars and SMM 2, 3 and 4; the emission to the NW, which covers the area encompassing SMM 1 (this is also called FIRS-1 by some workers), SMM 5 and 9; and a region in the NE of the map close to SMM 8. The CO lines have peak temperatures ~ 35 K close to SMM 4, but are more typically ~ 15 - 20 K elsewhere. Many of the CO profiles around SMM 1 and 4 are double peaked and appear to be self-reversed (see also Fig. 4 later), and the peak temperatures given above should be treated as lower limits.

In the NW corner, CO emission peaks ~ 25 arc seconds east and 20 arc seconds south of SMM 9, in a region where there is diffuse 1100 μm emission (Fig. 1g). This CO peak lies ~ 20 arc seconds east of the pre-stellar cloud S68N (McMullin et al. 1994). In Fig. 1e, a map of the $J = 4 - 3$ HCO$^+$ line peaks close to SMM 1, 3 and 4. This line has a high critical density ($\geq 10^6$ cm^{-3}), and traces denser gas than CO. The HCO$^+$ lines towards SMM 1 are all strongly self-reversed, and the peak temperatures are again lower limits - elsewhere the profiles are single peaked. A small map in the $^3P_1 - {}^3P_0$ CI line shown in Fig. 1f, has a peak close to SMM 1, and clumpy extended emission close to SMM 2 and 4. For comparison with the areas mapped in the molecular and atomic lines, the 1100 and 2.2 μm images (Casali et al. 1993) of the same area are shown in Figs. 1g and h. The main CO (and isotopomer) peaks lie to the East of the 2.2 μm ridge: the diffuse near-IR emission probably tracing the front edge of the cloud, with the CO ridge between the IR nebula and the C^{18}O and C^{17}O peaks (see also Fig. 6 later). The 2.2 μm ridge is dominated by the infrared emission of SVS 20, a pre-main sequence binary system and a nearby cluster of early stellar objects; the Northwest part of the map (where the 2.2 μm emission is much weaker) may be at an earlier stage of stellar formation (McMullin et al. 1994).

Channel maps for the CO and C^{18}O lines are shown in Fig. 2a and b.

The CO map is sharply peaked just north of SMM 4, with weaker emission extending to the E and NE of the map (close to SMM 3). Between 3 and 8 km s^{-1}, the emission comes mostly from the region close to SMM 4. There is little blue shifted gas close to SVS 2, which is suggests that it may have already emerged from the cloud edge, and material along the line of sight to it has already been dispersed. The CO is also extended to the SE and NW of SMM 4 towards SMM 2 and 3. The maps consist of relatively featureless widespread emission between 9 and 10 km s^{-1}, the structure being confused by the presence of widespread self-absorption. Between 11 and 18 km s^{-1}, the map is more complex, showing 6 or 7 hot-spots, the most intense lying close to SMM4. The lines are however strongly self-reversed, which may mask the true positions of the temperature peaks. The ^{13}CO map in Fig. 1b is very similar to that of CO at velocities close to the systemic velocity of the cloud (~ 7 - 8 km s^{-1}), indicating that both lines are relatively opaque - it is only for the rarer isotopomers that differences start to be seen, suggesting that they samplel material deeper into the cloud core.

The C^{18}O emission is confined to a narrower velocity range than the CO, extending across ~ 8 km s^{-1}, and the channel maps show peaks in different locations to those seen in CO, coming predominantly from south of the IR cluster, and from the northern complex. The lack of agreement between the CO and C^{18}O peak locations may suggest that the main CO peak near SMM 4 is hot gas that is externally heated (perhaps in a photodissociation region illuminated by the IR cluster stars), rather

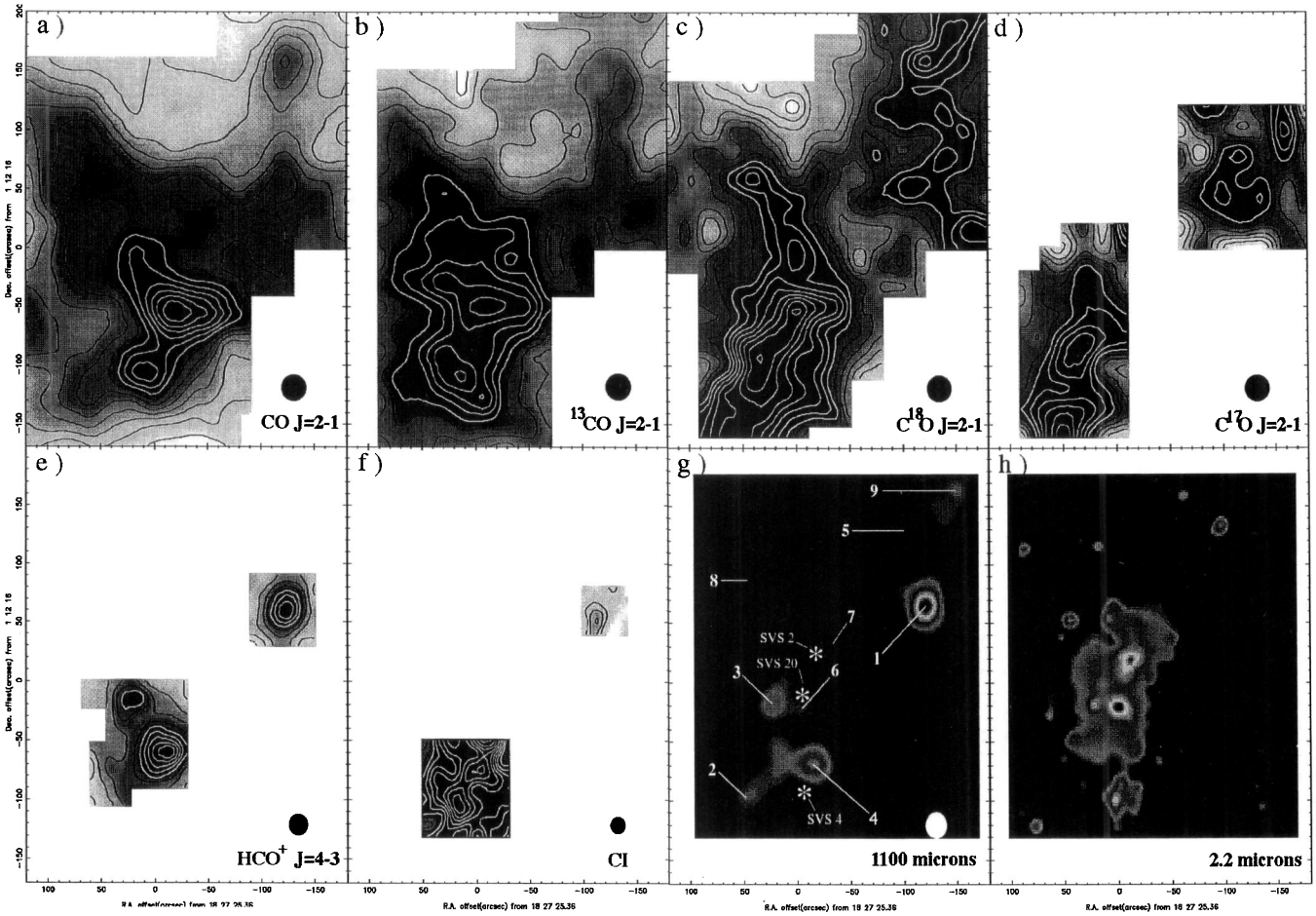

Fig. 1a–h. Maps of the $J = 2 - 1$ lines of **a** CO, **b** ^{13}CO, **c** C^{18}O and **d** C^{17}O, **e** the $J = 4 - 3$ HCO$^+$ and **f** the $^3P_1 - {}^3P_0$ carbon lines, and **g** the 2.2 and **h** 1100 μm emission adapted from Casali et al. (1993). The telescope beam sizes are indicated in the right hand lower corner as filled circles. The maps were integrated between velocities of -10 and 20 km s^{-1}, with values of the first contour, contour interval and first white contours for the line maps at **a** (50, 10, 120 K km s^{-1}), **b** (12, 3, 30 K km s^{-1}), **c** (2, 1, 9 K km s^{-1}), **d** (0.5, 0.5, 3 K km s^{-1}), **e** (2, 2, 18 K km s^{-1}), **f** (2.5, 2.5, 12.5 K km s^{-1})

than being excited by source(s) embedded inside the dense gas at the C^{18}O peak.

Emission from high velocity gas in the line wings is typically more than an order of magnitude weaker than the peak CO temperatures. In Fig. 3 a map of the high velocity gas (> 10 km s^{-1} from the cloud systemic velocity) is shown, superimposed on the 1100 μm map.

Regions showing high velocity (presumably outflow) gas lie close to SMM 1, 2, 3, 4, 8 and 9. The spatial structure of this high velocity emission is complex, and it is difficult to unambiguously associate the flows with individual SMM sources. It is however likely, based on the appearance of the map, that SMM 1, 2, 3, 4 and 8 individually drive outflow gas. SMM 9 (in the NW corner of the map) lies some distance from the nearest outflow gas, and it is possible that the compact core of S68N may be the driving source for this gas instead. However, McMullin et al. (1994) suggest that S68N is a condensation that has not yet begun significant star formation; unless the outflow phase has begun at a very early stage, S68N may not be the driving source. There is no common preferred direction for the outflowing gas; the orientation of the larger scale flow reported by Bally & Lada (1983) runs roughly SE-NW.

There is no high velocity gas that can be unambiguously associated with SVS 2, the dominant exciting star of the Serpens reflection nebula (at offset (-13, +25)). It is also unclear whether SVS 20 drives a flow, or that the nearby region of red and blue gas has been caused by the nearby SMM 3 - or SMM 4. It is however clear that multiple outflows are occurring contemporaneously within the core of the Serpens Nebula, suggesting that many stars are forming simultaneously.

CO spectra towards several of the SMM sources are shown in Fig. 4. These lie close to the centres of the prominent high velocity regions.

In all cases, the CO lines have two dominant velocities at $\sim$ 7 - 8 and 12 km s^{-1}, whereas the C^{18}O lines have peak velocities between 7 and 9 km s^{-1} and are always single peaked (the present data agree well with our earlier 55 arc second $J = 2 - 1$ observations of Serpens presented in Richardson

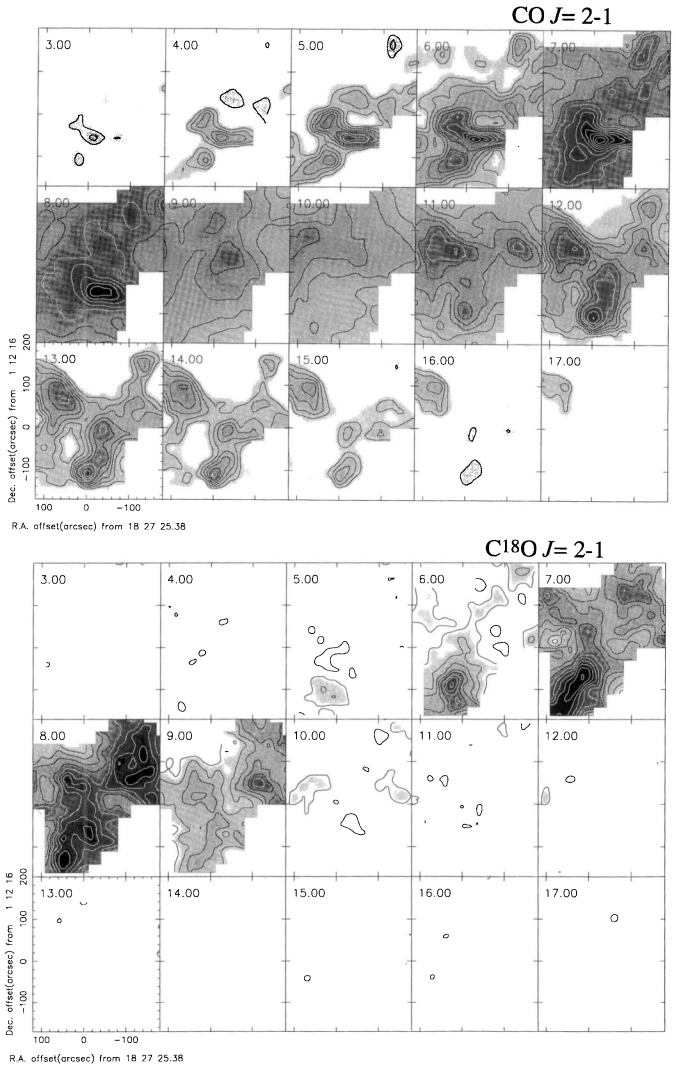

Fig. 2a and b. Channel maps for the CO and $C^{18}O$ $J = 2 - 1$ lines integrated in 1 km s^{-1} intervals. The lowest, interval and first white contours are **a** CO(4, 2, 28) K km s^{-1}, and **b** $C^{18}O$ (0.5, 0.5, 2.5) K km s^{-1}

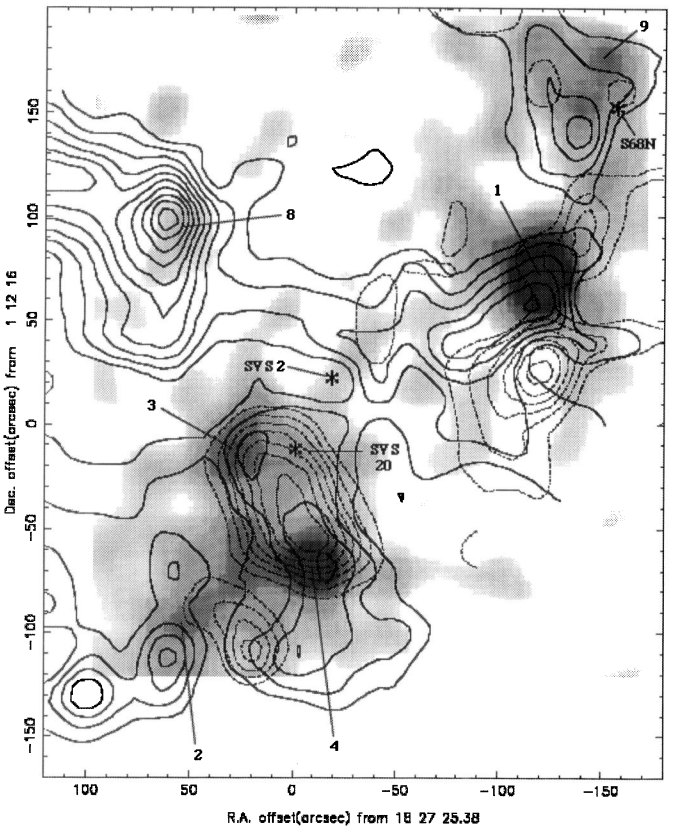

Fig. 3. Maps of the blue (-15 to - 2 km s^{-1} dashed lines) and red (17 to 40 km s^{-1} solid lines) high velocity gas superimposed on the 1100 μm continuum emission (grey scale). The contour levels for the red and blue shifted gas are in 2 K km s^{-1} steps, with the lowest contour at 4 K km s^{-1}. The numbers refer to the SMM sources shown on Fig. 1h, SVS 2 and 20 are near infrared sources first detected by Strom et al. (1976) and S68 is the position of a (pre-protostellar) molecular core noted by McMullin et al. (1994)

et al. 1985). The red shifted CO at velocities > 12 km s^{-1} is much weaker, and therefore probably optically thinner than the 7 - 8 km s^{-1} gas (probably explaining why the channel maps in Fig. 2a show more structure at 12 than at 7 - 8 km s^{-1}). Many of the spectra show a dip at ~ 10 km s^{-1}, which may be associated with self-absorption. The dip is always red shifted relative to the $C^{18}O$ line centre, suggesting the absorbing material lies along the line of sight to the sun. In most cases, there appears to be little absorption at the $C^{18}O$ velocity, giving some confidence that the peak CO temperatures may not be strongly affected by this effect. At the top of Fig. 4, all the CO, ^{13}CO, $C^{18}O$ and CI spectra were averaged together, to emphasise the highest velocity low-level gas from the region.

In Fig. 4, the $C^{18}O$ emission extends over the velocity range +4 and +12 km s^{-1} and the ^{13}CO from 0 to 18 km s^{-1} (compared with the total CO velocity range of ~ 70 km s^{-1}). There are deep absorption features in the $J = 2 - 1$ transition in the range 8 - 10 km s^{-1}, which are also seen in the $J = 1 - 0$ and $J = 3 - 2$ spectra of McMullin et al. (1994). The $C^{18}O$ $J = 2 - 1$ lines are slightly offset to the blue-shifted side of the absorption minimum. Such offsets have previously been reported towards other star forming regions, and interpreted as due to infall of the outer envelope of the cloud (Snell & Loren 1977). The velocity offset between the CO and $C^{18}O$ line peaks are particularly marked towards some positions (for example towards SMM 8), showing that the CO line profiles may sometimes be completely dominated by outflow emission whose opacity can not be particularly high.

The integrated CO line intensity in the high velocity gas outside the isotopomeric velocity range is 4.8 and 19.8 K km s^{-1} for the blue (+4 to -20 km s^{-1}) and red (+12 to +45 km s^{-1}) gas respectively. Assuming the CO outside the velocity range covered by the $C^{18}O$ is relatively optically thin (the ratios of the CO / ^{13}CO peak temperatures are typically > 20), then the method of Bachiller et al. (1990) can be used to obtain a first order estimate of the mass of material in the higher velocity ranges. We estimate lower limits to the masses of the red and blue high

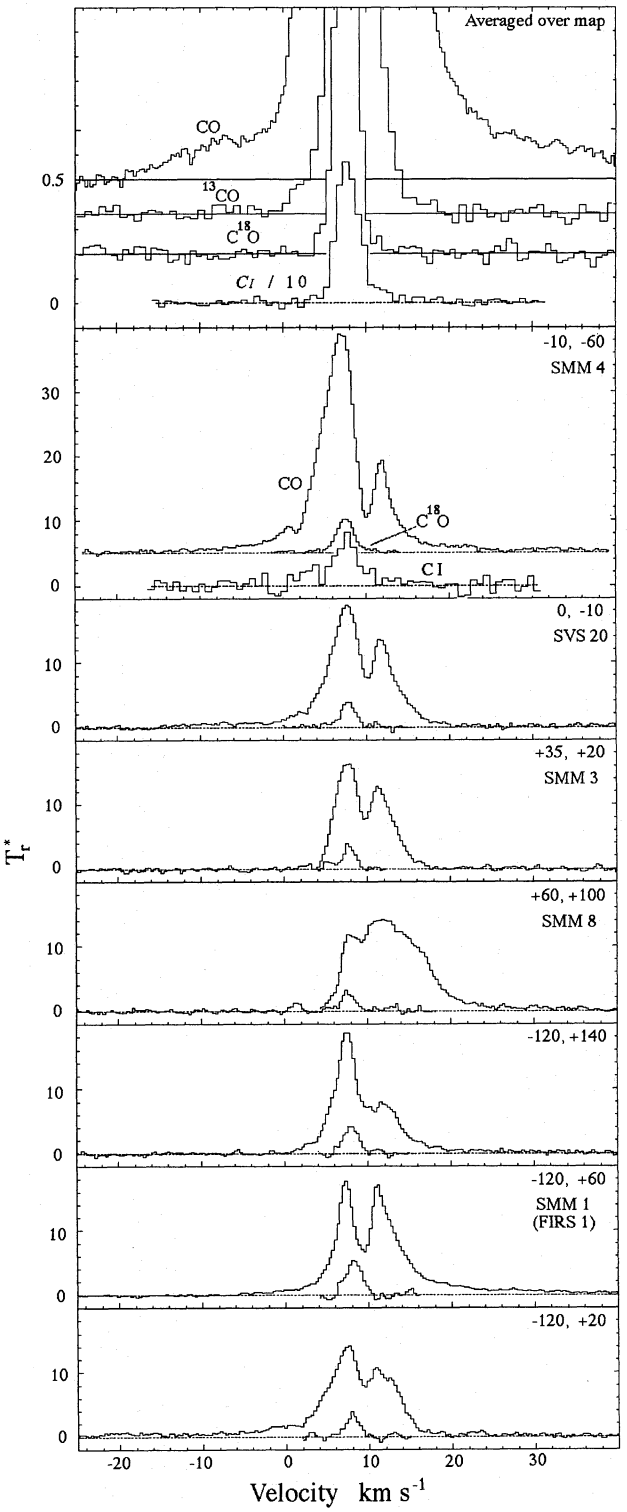

Fig. 4. CO and $C^{18}O$ spectra towards various positions in the cloud, and integrated across the whole mapped area. In all cases, the CO line is the stronger of the two. The top figure shows spectra integrated across the whole map (and includes the ^{13}CO spectrum), and the lower figures show spectra at individual positions. A spectrum in the CI line are also overlaid (for discussion see Sect. 3.5 on CI emission later). Note that the intensity scale of the averaged CI spectrum has been divided by a factor of 10

velocity gas to be $\sim$ 0.06 and 0.23 $M_\odot$, the momentum 0.42 and 1.53 $M_\odot$ km s^{-1} and the energy to be 4.8 10^{44} and 2.8 10^{45} erg s^{-1} respectively. Thus the high velocity gas at the centre of the Serpens region has characteristic properties lying between those typical of low luminosity outflows (such as L1551 - Parker et al. 1991), and of high-mass OB star formation regions. This is consistent with there being several overlapping flows which originate from individual low or intermediate mass star forming events. There is no evidence for a prominent outflow originating near the SVS 2 / Serpens reflection nebulosity, although there is some lower velocity gas which may be associated with the nearby $C^{18}O$ core. The flows are associated mainly with the more embedded or luminous objects (see Eiroa & Casali 1992 for discussion of intrinsic properties of the cluster's luminosity and extinction).

A remarkable alignment of the projected symmetry axes for a number of the optical objects and the triple radio continuum source along an SE-NW direction has previously been reported, parallel to the large scale helical component of the local magnetic field (Gomez de Castro et al. 1988). Eiroa & Casali (1989, 1992) have also found that the H_2 jet associated with SMM 1, as well as other extended infrared objects, lie along the same direction. It has been suggested that the magnetic field would play an important role in the morphology of the molecular outflows. From the distribution of the high velocity gas (Fig. 3), only the flow near SMM 1 is oriented along the same direction, whilst the rest of the outflow gas shows an extremely complicated morphology. There is little evidence in these molecular data that supports Gomez de Castro et al. 's suggestion that the molecular outflows should be co-aligned. There are a number of potential explanations; the poor agreement could for example result from an intrinsic lack of collimation, or that the flow directions are now not the same as they originally had - perhaps as a result of interaction with each other, or other ambient material. The present CO outflow maps seem to be too confused to resolve this issue.

The molecular outflow emission near SMM 1 is complex, with the blue high-velocity gas oriented along the jet-like H_2 emission associated with SMM 1. SMM 1 is a deeply embedded YSO and the most luminous object in the Serpens region (bolometric luminosity $\sim$ 80 $L_\odot$ - Casali et al. 1993). It has variable non-thermal radio emission (Curiel et al. 1993), and an associated jet-like nebulosity (mostly of H_2 emission), with a near-IR point source at its apex (Eiroa & Casali 1989; Casali et al. 1993). SMM 1 is most likely a 0.5 - 3 $M_\odot$ YSO, still shrouded within its placental material. The $C^{18}O$ data shows two peaks adjacent to SMM 1 (see Figs. 1c and 6a), these may be the limb-brightened edges of the elongated ridge reported by McMullin et al. (1994) from CS data. It is unclear from Fig. 3 whether there is just one pair of outflow lobes originating at SMM 1 (running SE-NW), or an additional pair (running N-S) which might suggest a more complex structure such as seen in L1551 (Rainey et al. 1987; Parker et al. 1991) and L723 (Avery et al. 1990).

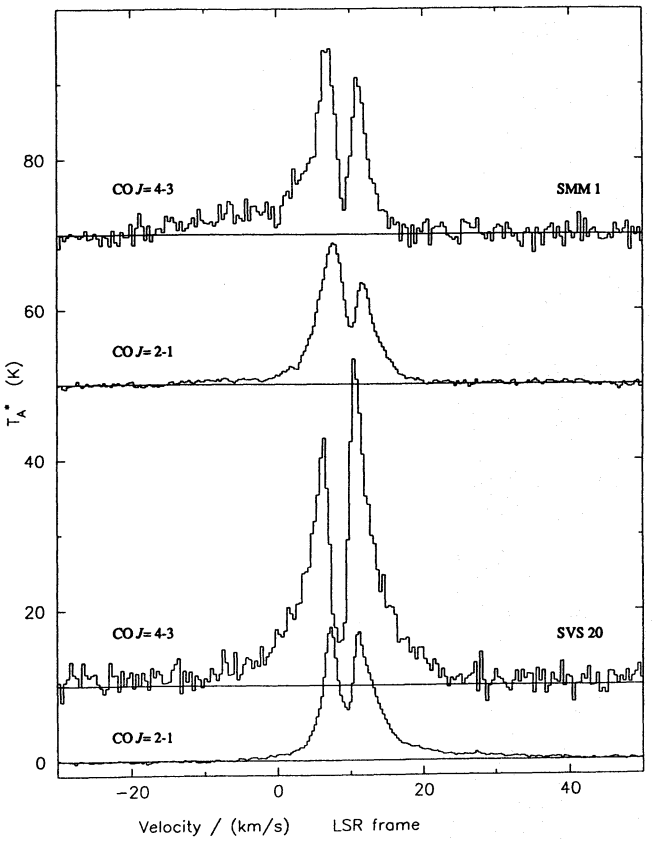

Fig. 5. CO $J = 2 - 1$ and $J = 4 - 3$ spectra towards SVS 20 and SMM 1. The $J = 4 - 3$ data have been convolved to same angular resolution as the $J = 2 - 1$ spectra

3.2. CO $J = 4 - 3$ data

Spectra in the CO $J = 4 - 3$ line obtained towards SVS 20 and SMM 1 are shown in Fig. 5.

Since the most intense CO peak is a small localised area, for inter-comparison with other lines we choose in this case to compare the main beam brightness temperatures. The peak main beam brightness temperatures at SVS 20 for the $J = 2-1$ ($\eta_{mb} = 0.58$) and $J = 4-3$ lines are similar; 25.5 and 25 K respectively - suggesting the gas is optically thick and thermalised at a kinetic temperature ~ 30 K. Towards SMM 1, the $J = 4-3$ brightness temperature is more intense; 24.0 and 45 K respectively, and has a deeper self absorption. The $J = 4-3$ spectra at both positions have intense broad wings: at SMM 1 extending between -10 and 25 km s^{-1}, and towards SVS 20, between -10 and 15 km s^{-1}. The strength of the $J = 4-3$ line confirms that this region may be warmer than quiescent dark clouds - not surprising in view of the external radiation field from the stellar cluster, and the embedded PMS objects. The values found in this work should be compared with the rotational temperatures ~ 30 K reported by Torrelles et al. (1992) from NH_3 observations.

3.3. $C^{18}O$ data

The $C^{18}O$ $J = 2-1$ peak temperatures are typically $\sim$ one quarter of the CO lines, suggesting opacities $\tau \geq 0.2$ in the highest column density regions (if the excitation temperatures are similar). $C^{18}O$ should therefore be a better tracer of the column density in the cloud core than for example the more optically thick ^{13}CO, although it is far from certain that $C^{18}O$ itself is completely optically thin. This is suggested by the fact that there are differences between $C^{18}O$ and the rarer $C^{17}O$ isotopomer maps (Figs. 1c and d), which may be attributable to opacity effects (see further discussion later).

The integrated $C^{18}O$ emission (Fig. 1c) peaks in the SE and NW sections of the mapped area. The individual $C^{18}O$ spectra are singly peaked with central velocities close to 8 km s^{-1}, except near to SMM 2, where the velocity is 6 - 7 km s^{-1}. Ungerechts & Güsten (1984) reported similar velocities from their NH_3 observations, suggesting a systematic velocity gradient of ~ 1 km s^{-1} across the cloud. The present $C^{18}O$ data do not give support for the presence of a systematic velocity gradient (which might indicate rotation); it is more likely that the velocities of individual clumps in the SE part of the map differ from the local systemic velocity of the source (~ 8 km s^{-1} for the non-moving quiescent gas) by up to a few km s^{-1}. The $J = 2 - 1$ $C^{18}O$ line widths are typically 2 - 3 km s^{-1}, with T_r^* towards the clump centres ~ 3 - 4.5 K. In Fig. 6a and b the integrated $C^{18}O$ map is superimposed on the 1100 and 2.2 μm maps of Eiroa & Casali (1992) and Casali et al. (1993), and in Fig. 6c onto the CO $J = 2 - 1$ map.

The main $C^{18}O$ ridge is offset ~ 1 arc minute south and east of the 2.2 μm emission nebula, but there is some correspondence with near-IR point sources close to 1100 μm sources SMM 1 and 4. The main $C^{18}O$ peak is in the region immediately to the East of the small southern cluster close to SVS 4 (at offset (-2,-94)). SVS 4 is itself a strong IR source with an associated radio continuum source (Rodriguez et al. 1980). It is surrounded by a cluster of ~ 11 other stars, in a region where the mass stellar density probably exceeds 1000 $M_\odot$ pc^{-3}. To the North of this, the $C^{18}O$ lies along a narrow ridge extending up towards SMM 4, stopping just to the East of it. Further north, $C^{18}O$ emission extends towards SMM 8, dropping off about 30 arc seconds south west of it. A weak peak is seen close to SVS 20. The strongest SMM source in the field, SMM 1, is straddled by two $C^{18}O$ peaks, linked to other emission stretching towards SMM 5 and 9.

The $C^{18}O$ ridge lies south of the infra red cluster. Weak $C^{18}O$ emission (stretching between SMM 4 and 8) lies superposed with the 2.2 μm cluster - although any direct association is unclear. The $C^{18}O$ enhancement close to SMM 1 contains two peaks located on either side of the continuum peak - which may be the limb-brightened edges of a disc (see Figs. 4c) and 6a). With the exception of the $C^{18}O$ peak at the position of CK 2 (one of the three most luminous sources in the cluster), the molecular structure is more closely correlated with the 1100 μm emission (with emission close to SMM 1, 4, 8 and 9) than the 2 μm distribution. This is consistent with the 2 μm cluster

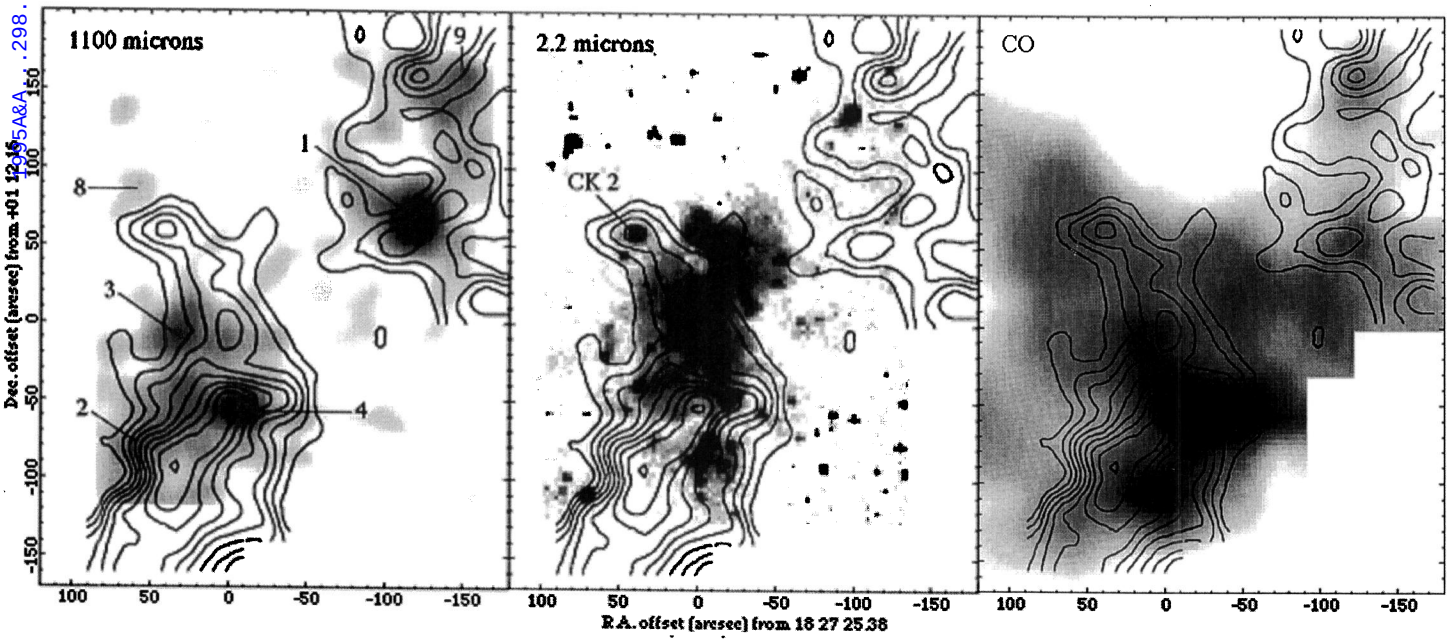

Fig. 6. a $C^{18}O$ map superimposed on the **a** 1100 μm and **b** 2.2 μm maps. The $C^{18}O$ contours run start at 8 K km s^{-1} (i.e. truncating the lower level emission), increasing in 1 K km s^{-1} intervals. In **c**, the $C^{18}O$ map is superimposed onto a grey scale image of the CO $J = 2 - 1$ map - shown originally in Fig. 1a

being an ensemble of young stars lying toward the front edge of the dense gas, whereas the SMM sources are more deeply embedded and intimately associated with the molecular gas.

The strongest peak in the CO $J = 2 - 1$ map is offset $\sim$ 10 arc seconds west of the $C^{18}O$ peak, coincident with SMM 4. Since there are weak wings on the $C^{18}O$ line extending between 4 and 12 km s^{-1} at this point (see Fig. 4), it is likely that the CO wing emission very opaque, with a low filling factor when observed with our beam. SMM 4 is strongly interacting with the surrounding material - providing heating and driving an outflow, whilst other embedded objects, such as SVS 20, does not appear to influence its surrounding so strongly. McMullin et al. (1994) suggest that the peaks of the CO and other higher excitation lines are close to SVS 20 - the present work suggests the SMM 4 region to be denser and more excited, and is consistent with McMullin et al. 's CS $J = 2 - 1$ map, which shows dense gas south of SVS 20. Other CO peaks lie to the SW of SMM 2, and close to SMM 8 and 9. Although there is CO in the area, there is no evidence that the 2.2 μm cluster is strongly heating the gas (for example in a photo dissociation region at the cloud's edge).

3.4. HCO^+ data

The HCO^+ map in Fig. 1e has three peaks, at SMM 1, 3 and 4, with the strongest emission at the latter position. The lines in the southern area of Fig. 1e are all single peaked, whereas towards SMM 1, are multiple, suggesting that HCO^+ is self absorbed. The CO and HCO^+ spectra around SMM 1 are shown in Fig. 7.

The self absorption dip shown above in the HCO^+ line is deepest at 8.7 km s^{-1} (close to that seen in the CO $J = 4-3$ line in Fig. 5), and slightly blue shifted from the CO $J = 2 - 1$ absorption minimum (at 9.5 km s^{-1}). The HCO^+ self-absorption appears much deeper than in the larger beam CSO spectrum of the same transition and position (McMullin et al. 1994), and is red shifted by $\sim$ 1 - 2 km s^{-1} . In comparison with the CO and HCO^+ data, and that of McMullin et al. (1994) there is a trend for the absorption minimum to move towards more blue shifted ve-

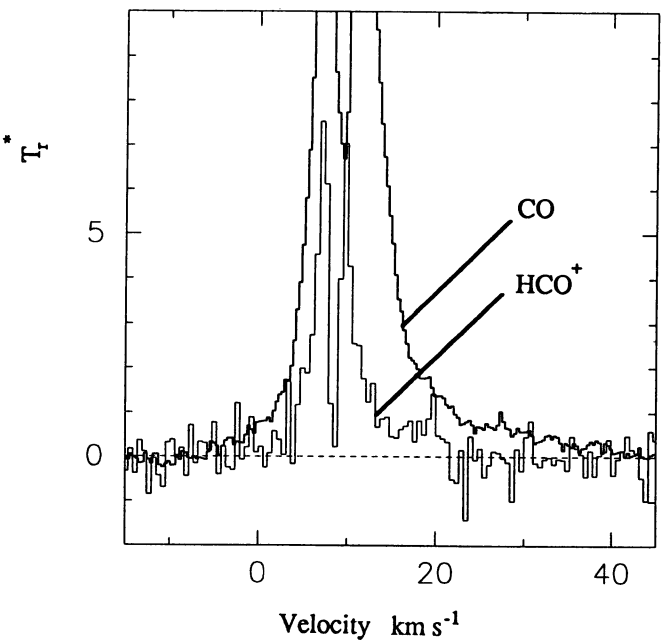

Fig. 7. a) HCO^+ $J = 4 - 3$ spectra around the position of SMM 1 (at -120, +60)

locities for the higher rotational transitions (when it is also blue shifted relative to isotopomeric lines). This would suggest that the self absorbing material contains significant structure (both spatially and kinematically) on a small size-scale, however this behaviour and the velocity separation from isotopomeric lines preclude a simple interpretation involving collapse alone. It is therefore clear that the thermal and velocity structure of material outside the core is complex, and that this source would be a good candidate for a future molecular line interferometric study (McMullin et al. 1994 also note that their CS data cannot be fitted with single density models).

There is also a low level HCO^+ wing extending out to ~ 20 km s^{-1}, which peaks at the (-120, 60) position, and is extended slightly to the North west. No significant blue wing counterpart was found. Although high velocity emission from HCO^+ has been seen toward other star-forming regions, the data are difficult to model and interpret due to the well-known problems of finite opacity, and sub-thermal excitation in this line (White et al. 1987). However, the present data do indicate a) there are density peaks close to the positions of SMM 1, 3 and 4, and b) that the outflow gas near SMM 1 contains some dense - presumably clumpy - material.

3.5. CI data

CI emission is widespread in the material to the SE and NW of the area mapped in $C^{18}O$ as shown in Fig. 1. The CI lines are single-peaked everywhere, but somewhat stronger ($T_r^* \sim 5$ - 7 K) in the SE (see Fig. 4 for an example) than the NW. T_{ex} (CI) ≥ 15 K in the SE and ≥ 10 K in the NW of the source. The CI peaks are not coincident with any of the ^{13}CO or $C^{18}O$ clumps - but appear more closely related to the CO emission, which has been noted to lie between the infrared cluster and the dense molecular ridge. This may suggest that both the CO and CI are excited in a photodissociation region along the edge of the ridge - but better signal to noise ratio data will be needed to confirm this.

The CI spectrum integrated over the whole mapped region was shown earlier in Fig. 4. The half power width is 3.6 km s^{-1}, and the peak intensity 5.7 K, with weak wings extending between 4 and 13 km s^{-1} (intermediate between the ^{13}CO and $C^{18}O$ widths measured to where they meet the noise). Fitting a gaussian to the CI wing emission we find $\int T_r^*\,dv = 3.9$ K km s^{-1}. Assuming $T_{ex} \sim T_{kin} = 20$ K (averaged over the map), the CI column density N_{col} (CI) (in units of cm^{-2} can be derived using the relationship;

$$N(CI) = 210^{15} \left\{ e^{\frac{23.6}{T_{ex}}} + 3 + 5e^{\frac{-38.0}{T_{ex}}} \right\} \frac{\tau}{(1-\exp(-\tau))} \int T_{mb} dv \quad (1)$$

For the integrated emission between 4 and 13 km s^{-1}, N_{col} (CI) is $\sim 5.6\ 10^{16}$ cm^{-2}. However the wing emission that does not appear merged with the narrow gaussian component (*i.e.* that not associated with ambient cloud material in the velocity range 10 and 13 km s^{-1}) has $\int T_r^*\,dv = 2.2$ K km s^{-1}, corresponding to N_{col} (CI) $\sim 3.2\ 10^{16}$ cm^{-2}. Integrating the ^{13}CO, $C^{18}O$ and $C^{17}O$ lines over the same velocity range gave values of $\int T_r^*\,dv = 3.92$, 0.22, < 0.03 K km s^{-1} respectively. The $C^{18}O$ line was used to set an upper limit to N(CO) of $\sim 1.5\ 10^{18}$ cm^{-2} (between 10 and 13 km s^{-1}, and assuming optically thin conditions with $T_{kin} = 20$ K and an abundance ratio $[CO]/[C^{18}O] = 500$ - see White & Sandell (1994) for a detailed discussion on CO isotopomeric abundance ratios). Hence we estimate $[CI]/[CO] \sim 0.02$ in this wing material, similar to values typical of shielded cloud material (White & Sandell 1994). Despite the (large) uncertainties, [CI] / [CO] is ~ 15 times less than in the S140 outflow (for which [CI]/[CO] = 0.28 as estimated by Minchin et al. 1994), and is consistent with the suggestion of Walker et al. (1993) that most high velocity CI emission seen so far is swept up ambient cloud material in which [CI]/[CO] is not strongly enhanced.

The CI column densities were calculated for the ambient cloud emission from the southern section of the CI map shown in Fig. 1f. The CI line intensities are relatively invariant, and N_{col} (CI) lies in the range ~ 1 - $7\ 10^{17}$ cm^{-2}, with an average of $4\ 10^{17}$ cm^{-2} (the data are shown later in Fig. 8). Due to this relatively small range, it is difficult to discern any correlation of CI column density with N(CO) or extinction A_v (see the next section for details on estimating these two quantities). The abundance ratio [CI]/[CO] = 0.2 ± 0.1. This is slightly higher than values now thought to be appropriate to material with A_v values ~ 10 - 20 (in comparison with the variations of the [CI] / [CO] ratio with A_v which have been reported by White & Sandell 1994 towards the Orion cloud, from which values of ~ 0.05 to 0.1 might be expected). To check the validity of the LTE approximation, we independently estimated the CO column densities using an LVG model for a cloud with a kinetic temperature of 40 K. Using the LVG derived column densities, the average value of [CI]/[CO] is 0.12 ± 0.06, which is now in reasonable agreement with the values obtained in the Orion cloud.

4. Column densities in Serpens

Molecular column densities of CO may be estimated using the emission from the $J = 2 - 1$ main isotope line and an optically thinner isotopomer, with the relationship;

$$N_{col} = \frac{6.9710^{15}}{\left[\frac{\nu}{GHz}\right]^2 \left[\frac{\mu}{Debye}\right]^2} T_{ex} e^{\frac{E_u}{kT_{ex}}} \frac{\tau}{1-e^{-\tau}} \int T_{mb} dV \quad cm^{-2} \quad (2)$$

where T_{ex} is estimated from the peak CO $J = 2 - 1$ main beam brightness temperature, $\int T_{mb}\,dv$ is the isotopomer's brightness temperature integrated over the line width, E_u is the upper state energy, ν is the line frequency, μ is the dipole moment and the opacity, τ, is estimated using the peak intensity of the line T_{peak} and the CO kinetic temperature T_{kin} is estimated from the relationship;

$$T_{peak} \cong \frac{h\nu}{k} \frac{(1-\exp(-\tau))}{\left(\exp\left(\frac{h\nu}{kT_{kin}}\right)-1\right)} \quad (3)$$

Equation 2 therefore assumes that the Planck corrected CO peak temperature is the same as the kinetic temperature (which is then assumed to be equal to the excitation temperature, and constant

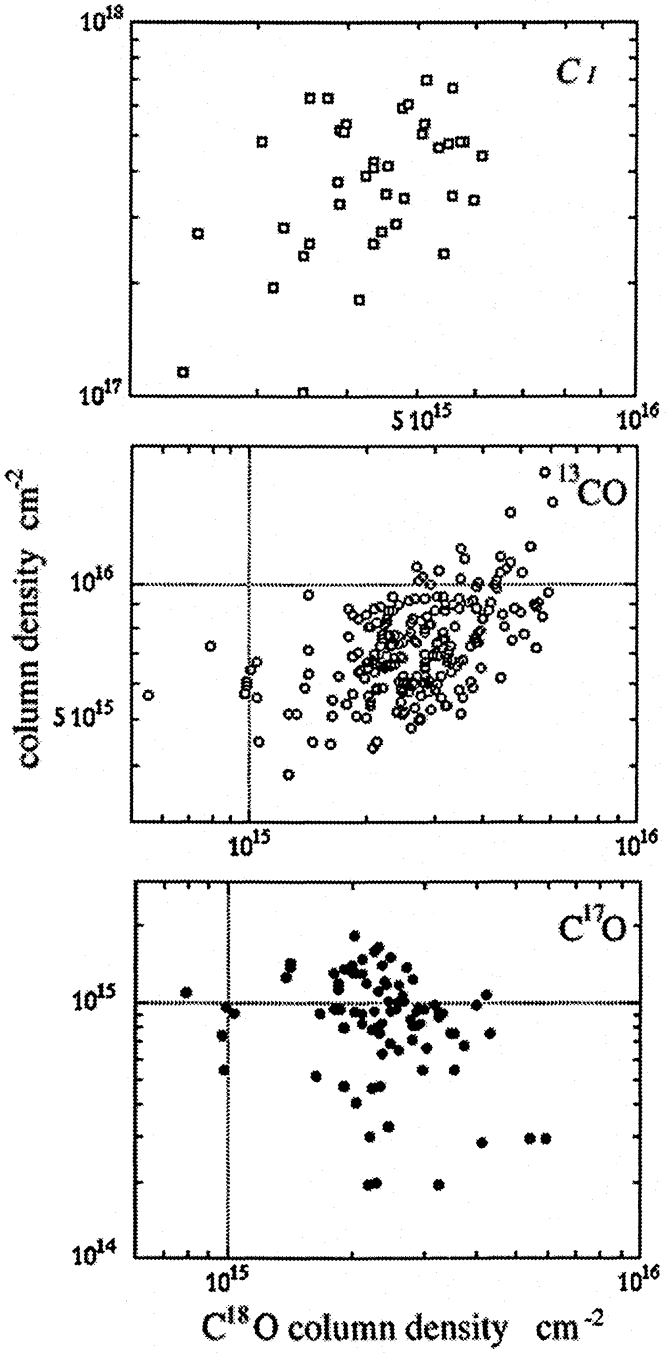

Fig. 8. Column density ratio estimates using the LTE approach with the data all treated in the same way as described in Eqs. 1), 2) and 3)

for all the CO rotational levels), that the isotopomer is in LTE, and that the escape probability:

$$\beta = \frac{\tau}{1-e^{-\tau}} \quad (4)$$

can accurately account for first order optical depth effects. In Fig. 8, the LTE column densities of ^{13}CO, C^{17}O and CI are plotted against those of C^{18}O.

This analysis (also referred to as the LTE method) is a 'standard' approach that has often been used for the interpretation of molecular line data; the estimation of cloud masses; and the inference of molecular abundances in the Interstellar Medium. Convenient qualifications are then often made to allow for the (usually unknown) uncertainties inherent in use of such a non-realistic simplification. In neither case (see Fig. 8) do the column densities of the isotopomers or CI show a good correlation with the C^{18}O column density.

This situation is quite different to that seen towards the hot Orion IRc2 star formation region, where C^{18}O and C^{17}O are both optically thin, and are closely correlated with each other, and with the (optically thin) 790 μm continuum emission (White & Sandell 1994). It appears likely that LTE column density estimates using ^{13}CO and C^{18}O data towards Serpens are unreliable, and so possibly are those estimated from the rarer isotopomer C^{17}O. Monte Carlo calculations of several other dark clouds (Avery et al. 1987) have already shown that the $J = 2 - 1$ and $J = 3 - 2$ CO transitions are sub-thermally excited, and that the cloud cores may be hidden by a surrounding lower density envelope. This means that although the most optically thin lines (such as C^{17}O) trace emission from the denser regions at the core, the column densities derived using LTE techniques may be unreliable - particularly in low density cool regions.

The data shown in Fig. 8 can also be presented in a way that has been used in the past, as evidence for isotopic fractionation - see Fig. 9,

Figure 9 appears at first sight to show strong evidence for the enhancement of both densities (relative to C^{18}O and C^{17}O respectively) in the less shielded parts of the cloud. The behaviour seen in Fig. 9 is however at variance with that found by White & Sandell (1994) towards Orion, where only ^{13}CO shows evidence for enhancement - in line with theoretical understanding (van Dishoeck & Black 1988; Köster et al. 1994). It therefore seems likely that the effects seen in Fig. 9 are a consequence of the failure of the LTE method to give useful column densities, rather than due to isotopomeric enhancement of both the ^{13}CO and C^{18}O. Alternatively, the trends may be indicative of optical thickness of C^{18}O at higher column densities, which may be a consequence of clumping on smaller size scales than the beam size.

To examine this problem further, LVG calculations were performed for clouds with kinetic temperatures of 10 K and 20 K, to obtain the column density that would be estimated for various antenna temperatures. These values are slightly lower than seen towards the warm cores in Serpens, but are probably more representative of the emission from the bulk of the cloud ensemble, towards which most of the data shown in Figs. 8 and 9 refer (see also Sect. 3.1). The H_2 particle density, N(H_2) was set to values of 10^3 and 10^4 cm^{-3}, and column densities calculated for the C^{18}O antenna temperature range observed towards Serpens ($\sim$ 0.5 - 5 K). Column density estimates for the $J = 1 - 0$, $J = 2 - 1$ and $J = 3 - 2$ transitions were then compared with values derived using the relationships in the LTE equations (1) and (2), and shown in Fig. 10a, b and c below.

These calculations show that column densities estimated by the LTE model differ by perhaps one order of magnitude compared to those inferred using an LVG model for the cases of

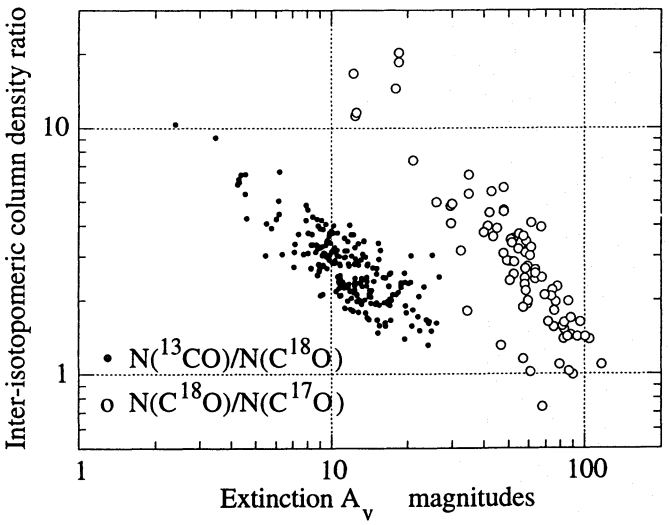

Fig. 9. Column density ratios plotted against extinction. The extinctions for the $^{13}CO/C^{18}O$ data were obtained using the $C^{18}O$ data and Lada et al. 's (1994) relationship $N(C^{18}O)/A_v = 2.29\ 10^{14}\ cm^{-2}\ mag^{-1}$. For the $C^{18}O/C^{17}O$ data we used the $C^{17}O$ data, and scaled Lada et al. 's relationship by an additional factor of 3.5 (so that $N(C^{17}O)/A_v = 6.54\ 10^{13}\ cm^{-2}\ mag^{-1}$) to get a first order estimate of the extinction values for the $C^{18}O/C^{17}O$ data. The graph suggests that $C^{17}O$ is preferentially emitted by larger A_v material (or that Lada et al. 's relationship cannot be reliably extrapolated)

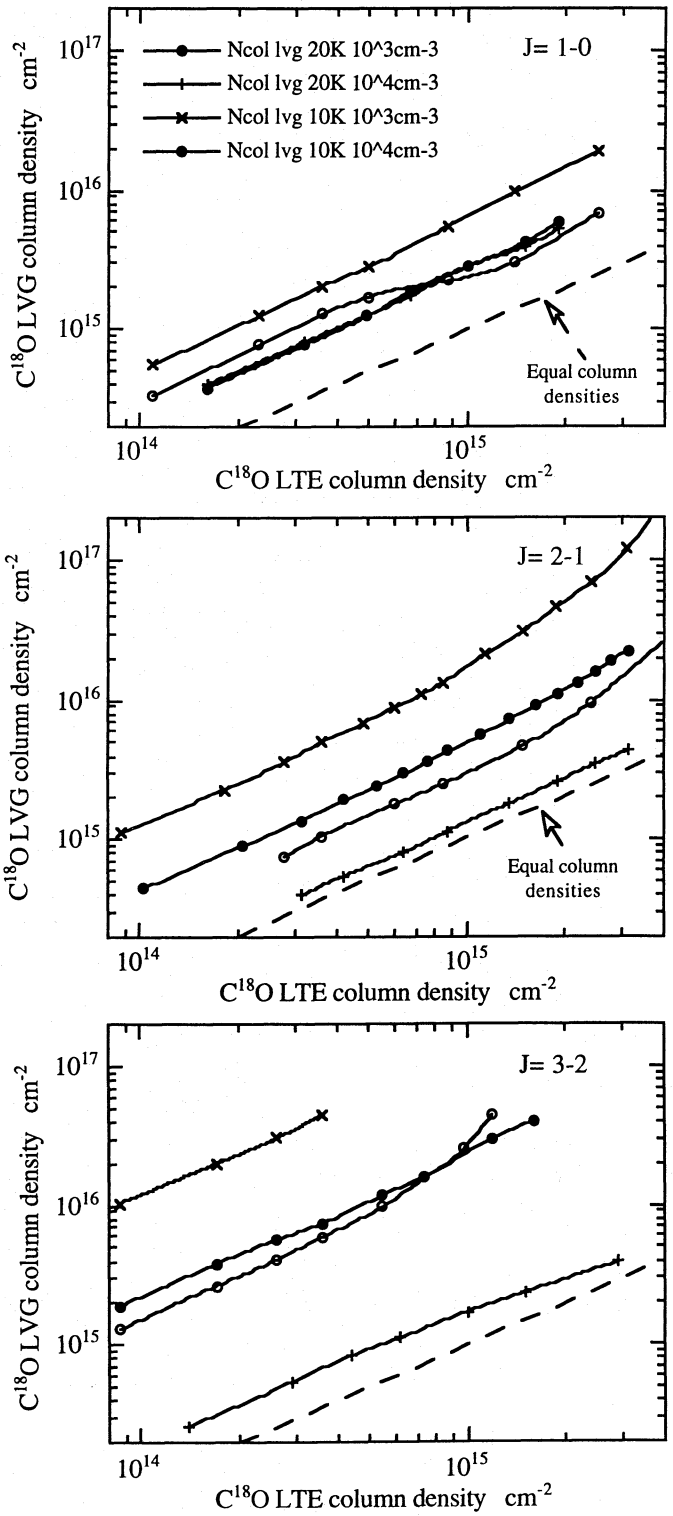

Fig. 10. Comparison of $C^{18}O$ $J = 1 - 0$, $J = 2 - 1$ and $J = 3 - 2$ column densities derived using LVG and LTE techniques. The LTE estimates are consistently lower, by factors of 4 - 70, of those indicated by the LVG analysis. The points indicated on the curves have no significance - they were just used to define the shape of the fits

low density cool gas (see also discussion by Richardson et al. 1985). In all cases, the column densities are lower than those in the LVG calculation. This result is consistent with sub-thermal excitation of the $C^{18}O$ lines, as has been previously suggested by our previous Monte Carlo modelling (Avery et al. 1987), towards dark clouds observed in the $J = 2 - 1$ and $J = 3 - 2$ transitions. This modelling suggested that the cores are often surrounded by lower density envelopes, which can modify the line shapes and temperatures due to material in the core. Schilke et al. (1994) have subsequently arrived at similar conclusions towards the Taurus dark cloud core TMC-1. The discrepancies between LTE and LVG estimates are more pronounced at the lower densities and temperatures found in dark clouds, than towards warmer clouds (where most of the published $C^{18}O$ observations to date have been made). This is consistent with the suggestion of Richardson (1994) that the LTE method is only effective at estimating column densities (at the centre of a line) down to an optical depth of $\sim$ unity.

The LVG column densities for the $J = 2 - 1$ lines are $\sim$ 4 - 8 times, and $\sim$ 12 - 70 times greater than the LTE estimates, for kinetic temperatures of 20 and 10 K respectively. Figure 10 also shows a similar calculation for the $J = 1 - 0$ and $J = 3 - 2$ $C^{18}O$ lines, where a similar trend is seen. The difference between LVG and LTE estimates is greatest at the

higher J- transitions and in cooler material. Despite the problems highlighted above in reliably estimating column densities, it has been a widespread practice amongst many molecular line astronomers to use the LTE optically thin approximation. It is likely that LTE based estimates of dark cloud masses using the higher rotational transition $C^{18}O$ lines to estimate column densities, will under-estimate the true masses. Mass estimates using the ^{13}CO lines are even more unreliable, due to the finite opacity in this isotopomer. However, in the warm (> 20 K) moderate density ($> 10^4$ cm^{-3}) gas in the central region of the Serpens Nebula, the LTE and LVG estimates agree more closely.

4.1. Mass of the region and the star formation efficiency

A lower limit to the mass of material (subject to the caveats and uncertainties discussed above) can be estimated using the CO, and an optically thin isotopic line, making first order corrections for opacity. This estimate assumes $[C^{18}O]/[H_2] = 2.3\ 10^{-7}$ and $[C^{17}O]/[H_2] = 6.6\ 10^{-8}$ (as discussed earlier), that the isotopes are optically thin and have a similar excitation temperatures to CO, and that the distance to the Serpens Nebula is 311 pc (De Lara et al. 1991). As discussed in the previous section, mass estimates derived in this way, although having been 'standard' practice in many previous studies of molecular clouds, may be very uncertain - and true cloud masses may be higher than the estimates indicate. For the whole area shown in Fig. 1c, we estimate a lower limit on the molecular gas of 1450 $M_\odot$ from the $C^{18}O$ data, and 400 $M_\odot$ for the area shown in Fig. 1d from the $C^{17}O$ data. These values should be compared to the 420 $M_\odot$ estimated for the central 3.3 arc minutes around the core, by Loren et al. (1979) using ratios of the 2 cm and 2 mm H_2CO lines (i.e. for the densest parts of an area ~ 40 percent of that covered by the $C^{18}O$ observations).

The star formation efficiency (SFE) to date for the region can be estimated using the relationship;

$$SFE = \frac{M_{stars}}{M_{gas}+M_{stars}} \quad (5)$$

The mass of stars associated with Serpens have been estimated by Eiroa & Casali (1992) to be ~ 37 $M_\odot$ (assuming stellar luminosity / mass assignments according to Sect. 3.8 (a) from Eiroa & Casali (1992) - although these are difficult to do determine accurately since the luminosities of pre main sequence stars may change with time). From the $C^{18}O$ estimated mass, we set an upper limit of the SFE of ~ 2.5 percent. This is comparable with that estimated towards other dark cloud complexes; Ophiuchus :- 0.8 percent (Wilking et al. 1989); Taurus :- 0.7 percent (Kenyon et al. 1990); L1641 :- 0.6 percent (Evans & Lada 1991); L1630 :- 3 to 4 percent (Lada 1990). It is important to note that these are lower limits to the final value of the SFE of a cloud - they just reflect the star forming activity that has occurred to date (Evans et al. 1991; Leisawitz et al. 1989).

The value of 2.5 percent is lower that estimated using the Loren et al. (1979) data, most likely because the H_2CO preferentially will trace higher density material from the central core. However, other mass estimates of dense gas by Ungerechts & Güsten (1984) (for NH_3 and H_2CO) are as low as ~ 10 $M_\odot$. Since NH_3 traces denser gas than $C^{18}O$, we take the NH_3 estimates only as a lower limit. Loren et al. 's (1979) observations were made with large beams, and may have an uncertainty of a factor of 3 - 5 for the estimated mass due to uncertainties in radiative transfer effects and geometry. The disagreement with the more recent Ungerechts & Güsten (1984) H_2CO results, show that significant differences still remain (in the interpretation as well as the data).

The mass estimated from the present $C^{17}O$ data is ~ 400 $M_\odot$, which although agreeing more closely with the H_2CO estimate, refers to a smaller area, and must again be seen as a lower limit. As has been argued earlier, it is likely that $C^{18}O$ (and similarly $C^{17}O$) data will result in under-estimates of the cloud mass. There seems to be little evidence to support the suggestion that the SFE could be as high as 28 percent (Eiroa & Casali 1992); it is probably no more than several percent.

5. Conclusions

The Serpens nebula is in the final stages of forming cluster of stars. Only a small percentage of the gas in the cloud core has been converted into stars, and evidence of active and ongoing star formation is present. The $C^{18}O$ mass is ~ 1450 $M_\odot$, implying that the star formation efficiency within the mapped region around the Serpens Nebula is ~ 2.5 percent (or less) to date.

There is a considerable amount of molecular outflow activity occurring, identifiable both as discrete outflows around specific SMM sources (1, 2, 3, 4, 8, and perhaps 9) as well as more widespread diffuse high velocity gas that is present over much of the area. The mass and energy of material in the high velocity gas are relatively small, ~ 0.3 $M_\odot$ and 3 x 10^{45} erg s^{-1}, consistent with there being a number of overlapping flows having characteristics typical of those seen towards lower mass star-formation regions. There is little evidence to support the suggestion that the majority of the outflowing gas lines up along the large scale magnetic field direction (Gomez de Castro et al. 1988), or that the flows share some common orientation.

The gas temperatures in the central regions are warmer ($\sim$ 30 - 40 K) than those seen in dark clouds, suggesting that the Serpens cluster has heated the gas considerably. The hottest CO lies towards the edge of the higher column density material, along the direction towards the more luminous near infrared sources.

Attempts to study the relative isotopomeric abundance ratios in this source are severely hampered by opacity, uncertainty of the radiative transfer, and excitation effects - the inferred column densities possibly being uncertain by up to an order of magnitude, depending on the analysis technique used.

Acknowledgements. The UK Science & Engineering Research Council is thanked for supporting the Submillimetre Wave astronomy and instrumentation programme at QMW. The JCMT is operated by the Royal Observatory, Edinburgh on behalf of the UK Science & Engineering Research Council, The Netherlands Organisation for Scientific Research and the Canadian National Research Council. The Royal So-

ciety are thanked for support from their Research Grant Scheme which provided Image Processing Equipment needed for the data analysis. We acknowledge discussions with Gary Fuller and Ned Ladd about their unpublished CS and CO isotopomeric observations of this source, and thank J. McMullin for sending his preprint. The referee is thanked for an excellent review of the manuscript and suggestions which led to improvements and clarifications.

References

Avery, L.W., White, G.J., Williams, I.P. and Cronin, N. 1987, ApJ, 312, 848.
Avery, L.W., Hayashi, S.S. and White, G.J. 1990, ApJ, 357, 524.
Bachiller, R., Cernicharo, J., Martin-Pintado, J., Tafalla, M. and Lazareff, B. 1990, A&A, 231, 174.
Bally, J. and Lada, C.J. 1983. A&A, 265, 824.
Casali, M.M., Eiroa, C. and Duncan, W.D. 1993, A&A, 275, 195.
Curiel, S., Rodríguez, L.F., Moran, J. and Cantó, J. 1993, ApJ, 415, 191.
De Lara, E., Chavarria-K, C., Lopez Molina, G. 1991, A&A, 243, 139.
Eiroa, C. & Casali, M.M. 1989. A&A, 223, L17.
Eiroa, C. 1991, p197 'Low Mass Star Formation in Southern Molecular Clouds', ESO
Eiroa, C. and Casali, M.M. 1992, A&A, 262, 248.
Eiroa, C., Torelles, J.M. and Gomez, J.F., 1992, PASJ, 44, 155.
Evans, N.J. and Lada, E.A. 1991, 'Fragmentation of Molecular Clouds and Star Formation', IAU Symposium 147, p293, D. Reidel Press.
Gomez de Castro, A.I., Eiroa, C. and Lenzen, R. 1988, A&A, 201, 299.
Harvey, P.M., Wilking, B.A. and Joy, M. 1984, ApJ, 278, 156.
Kenyon, S.J., Hartmann, L.W., Strom, K.M. and Strom, S.E. 1990, AJ, 99, 869.
Köster, B., Störzer, H., Stutzki, J. and Sternberg, A. 1994, A&A, 284, 545.
Lada, E.A. 1990, PhD Thesis, University of Texas at Austin.
Lada, C.J., Lada, E.A., Clemens, D.P. and Bally, J. 1994, ApJ, 429, 694.
Lada, C.J., Lada, E.A., Clemens, D.P. and Bally, J. 1994, ApJ, 429, 694.
Leisawitz, D., Bash, F. and Thaddeus, P. 1989, Ap J Suppl, 70, 731
Loren, R.B., Evans, N.J. and Knapp, G.R. 1979, ApJ, 234, 932.
McMullin, J.P., Mundy, L., Wilking, B.A., Hezel, T. and Blake, G.A. 1994, ApJ, 424, 222.
Minchin, N.R., White, G.J., Stutzki, J. and Krause, D. 1994, A&A in press.
Nordh, H.L.,van Duinen, R.J.,Sargent, A.I. et al., 1982, A&A, 115, 308.
Parker, N., White, G.J., Hayashi, S. & Williams, P.G. 1991, A&A, 250, 134
Rainey, R., White, G.J., Richardson, K.J., Griffin, M.J., Cronin, N.J., Monteiro, T.S. and Hilton, J. 1987, A&A, 179, 237.
Richardson, K.J., White, G.J., Avery, L.W., Lesurf, J.C. and Harten, R.H. 1985, ApJ, 290, 637.
Richardson, K.J. 1994, Preprint
Rodriguez, L.F., Moran, J.M., Ho, P.T.P. and Gottlieb, E.W. 1980, ApJ, 235, 845
Schilke, P., Keene, J. and Le Bourlot, J. 1994, Preprint.
Snell, R.L. and Loren, R.B. 1977, ApJ, 211, 122.
Strom, S.E., Vrba, F.J. and Strom, K.M. 1976, AJ, 81, 638.
Torrelles, J.M., Gomez, J.F., Curiel, S., Eiroa, C., Rodriguez, L.F. and Ho, P.T.P. 1992, ApJ, 384, L59.
Ungerechts, H. and Güsten, R. 1984, A&A, 131, 177.
van Dishoeck, E. F., and Black, J.: 1988, ApJ., 334, 771.
Walker, C.K., Narayanan, G., Büttgenbach, T.H., Carlstrom, J.E., Keene, J. and Phillips, T.G. 1993, ApJ, 415, 672.
White, G.J., Rainey, R., Hayashi, S.S. and Kaifu, N. 1987, A&A, 173, 337.
White, G.J. 1988. 'Millimetre and Submillimetre Astronomy', p 27-94, ed. Wolstencroft, R.D. and Watt, G.D. Kluwer Academic Publishers.
White, G.J. and Sandell, G. 1994, A&A submitted.
Wilking, B.A., Lada, C.J. and Young, E.T. 1989, ApJ, 340, 823.
Zhang, C.Y., Laureijs, R.J. and Clark, F.O. 1988, A&A, 196, 236.

This article was processed by the author using Springer-Verlag LaTeX A&A style file version 3.